Research Square

Preprints are preliminary reports that have not undergone peer review.
They should not be considered conclusive, used to inform clinical practice,
or referenced by the media as validated information.

Performance and degradation mechanism analysis of grouting and coating epoxy material in Cave 16 of the Yungang Grottoes

Shangxiao Qiao
Yungang Academy
Qi Wang
Yungang Academy
Ding Yan
Yungang Academy
Xiang He
Hexiang@ustb.edu.cn

Key Laboratory of Archeomaterials and Conservation, Ministry of Education
Xue Bai
Yungang Academy

Article

Keywords: Yungang Grottoes, epoxy resin, coating material, grouting material, deterioration mechanism, stone heritage conservation

Posted Date: June 15th, 2026

DOI: https://doi.org/10.21203/rs.3.rs-9895661/v1

License: This work is licensed under a Creative Commons Attribution 4.0 International License.
Read Full License

Additional Declarations: No competing interests reported.

Abstract

The epoxy-based coating and grouting materials applied in Cave 16 of the Yungang Grottoes during the Three-year Conservation Project (1974–1976) have been in service for approximately 50 years. However, their current condition, extent of deterioration, and degradation mechanisms remain poorly understood. Field samples of detached surface coating and grouting materials were collected from Cave 16, and simulated samples were prepared using epoxy 6101 in accordance with historical conservation records. Microscopic observation and nanoindentation revealed darkening and hardness decrease among the field samples. TGA and FTIR analysis indicated that degradation leads to the loss of isopropyl groups, an increase in carbonyl functionality, and diminished aromaticity. The natural degradation products included aliphatic polymeric residue, and carboxylate species; the formation of carbonyl groups contributed to the observed darkening. It is concluded that the degradation of the epoxy materials involves oxidation, isopropyl group rearrangement and cross-linking. Notably, the coatings exhibited more severe degradation than the grouting materials, attributable to their greater exposure to oxygen and light. This study elucidates the degradation mechanisms of the epoxy coating and grouting materials in Cave 16, providing a scientific basis for optimizing conservation materials and strategies in caves and offering practical guidance for the preservation of analogous cultural heritage sites.

1.Introduction

The Yungang Grottoes, designated as a UNESCO World Heritage Site of outstanding universal value and among the first batch of key cultural relics units under national protection, was carved during the Northern Wei Dynasty (Fig. 1(a)). The site is renowned for its murals and Buddhist sculptures, which embody multi-ethnic and multicultural characteristics and represent the pinnacle of northern Chinese Buddhist art. Cave 16 is distinguished as the only cave featuring musical imagery among the five Tanyao caves (Fig. 1(b)), containing numerous exquisitely carved musical instruments of significant historical, artistic, scientific, and cultural value [1]. Consequently, the scientific conservation of this site constitutes both a national obligation and an undertaking of global significance.

Epoxy resin represents one of the most important organic conservation materials for stone cultural heritages. Since the mid-twentieth century, epoxy resins have been extensively applied owing to their favorable workability and high adhesive strength, despite drawbacks, including the migration of components and their subsequent surface enrichment upon solvent evaporation [2], as well as susceptibility to degradation and discoloration under ultraviolet radiation and humid-thermal degradation. Such degradation phenomena have been documented at the Katsura Imperial Villa in Japan, the Church of Santa Maria dei Miracoli in Italy, and at the Longmen and Yungang Grottoes in China [3, 4].

The conservation interventions carried out five decades ago have yielded invaluable samples for investigating the long-term in-service performance of these materials. In the early 1970s, bonding tests were conducted at the Yungang Grottoes, during which suitable grouting materials were injected into

fractures within the surrounding rock. Subsequently, during the Three-year Conservation Project (1974–1976), an epoxy resin-furfural-acetone-amine system was employed for large-scale emergency stabilization of the caves [5]. This initiative marked one of the earliest large-scale applications of epoxy resin for the reinforcement of stone cultural heritage worldwide [6]. It substantially alleviated the severe water-infiltration problem that had been accelerating the deterioration of the caves. Nevertheless, the current condition of these materials after prolonged degradation remains unclear and must be assessed to inform future conservation planning.

An understanding of deterioration mechanisms is essential for guiding the modification of conservation materials. The thermal oxidative degradation of epoxy resins is generally understood as a free-radical chain reaction involving initiation, propagation, and termination stages. Molecular oxygen attacks tertiary carbon atoms in isopropyl groups or abstractable hydrogens along the backbone, generating alkyl radicals that rapidly convert to hydroperoxides (ROOH) [7]. The chain breakage in epoxy resin mainly occurs at the C–O bond [8], producing low-molecular-weight fragments products such as isopropanol and bisphenol A. Subsequently, isopropanol is oxidized to generate carboxylic acid [9], while the phenoxy group in bisphenol A is oxidized to phenyl formate, which further decomposes after ester bond cleavage to produce carbon dioxide [10]. Isopropyl groups, owing to the high activity of their tertiary carbon atoms, readily form free radicals in the presence of oxygen, leading to a series of reactions that generate ketones and other substances [11].

However, the history of epoxy resin as a heritage conservation material remains relatively short, and studies on its long-term degradation mechanisms—especially those based on field samples—are scarce. Tesser et al. prepared simulated samples using epoxy EP2101 and subjected them to 12 months of natural degradation and 1250h of accelerated artificial degradation. Their results indicated that light is the primary factor in epoxy degradation; ultraviolet radiation triggers free radical reactions generating alkyl radicals and forming carbonyl groups through molecular chain scission, resulting in degradation and darkening of epoxy resin. Nevertheless, this mechanism is based on photodegradation and is therefore not directly applicable to the low-light environment of grottoes, particularly for grouting materials located within rock fractures [12].

Given the lack of understanding regarding the long-term degradation behavior of epoxy resins in heritage conservation—especially under the low-light, high-humidity conditions typical of cave temples— this study focuses on the epoxy grouting and coating materials applied in Cave 16 of the Yungang Grottoes during the 1974–1976 conservation campaign. Field samples of epoxy resin aged for approximately 50 years were collected, and their microstructural, mechanical, and chemical characteristics were analyzed using multiple analytical techniques. Simulated samples were also prepared for reference. By identifying and characterizing the degradation products, this study elucidates the deterioration mechanisms of these historical conservation materials, thereby providing a scientific basis for the future conservation of the Yungang Grottoes and the development of conservation materials for stone heritage.

2. Materials and methods

2.1. Materials

In 2025, on-site sample collection was carried out on the first and second floors of the scaffolding inside Cave 16 of the Yungang Grottoes. Scattered rock debris, surface coating materials, and grouting materials were collected using tweezers from the grouting areas and the ground. All samples had already detached or were on the verge of detaching from the grotto wall surfaces, as shown in Table 1.

Simulated samples were prepared based on internal documents of the 1974–1976 rescue and reinforcement project from the Yungang Research Institute. Historical records indicate that this project is the sole application of epoxy-based materials for the reinforcement of Cave 16. According to these records, both the coating and grouting materials were formulated within an “epoxy resin–furfural–acetone–amine” system, in which furfural and acetone functioned primarily as viscosity reducers and permeability enhancers, while the amine served as the curing agent. The weight ratios for the grouting and coating materials were 10:2:2:2 and 10:1:1:0 (epoxy resin 6101: acetone: polyethylene polyamine: furfural), respectively (Table 1). Actual proportions varied according to specific on-site application requirements. The simulated samples were prepared using epoxy resin 6101 (Macklin, Shandong Keyuan Biochemical Co., Ltd.), acetone (Shanghai Zhanyun Chemical Co., Ltd.), polyethylene polyamine (Macklin, Shandong Keyuan Biochemical Co., Ltd.), and furfural (Shanghai Zhanyun Chemical Co., Ltd.). The simulated grouting and coating samples were cured at room temperature.

Table 1
List of test samples

	Number	Sample category	Sampling or sample preparation information
Field samples	YG-1	Grouting	On the middle section of the east wall, approximately 12 m above ground level.
	YG-3	Coating	At main Buddha's left arm, approximately 12 m above ground level.
	YG-4	Grouting	At corners and edges of the grotto clerestory, approximately 12 m above ground level.
	YG-5	Rock fragments	From a fallen rock block on the east wall.
	YG-6	Rock fragments	At the foot of the Buddha on the east wall.
	YG-7	Coating	On the left shoulder of the Buddha in the middle of the south wall, approximately 8.5 m above ground level.
Simulated samples	MN-1	Coating	Filler (calcium carbonate): epoxy 6101: acetone: polyethylene polyamine: furfural = 10: 10: 1: 1: 0
	MN-4	Coating	epoxy 6101: acetone: polyethylene polyamine: furfural = 10: 1: 1: 0
	MN-5	Grouting	Filler (calcium carbonate): epoxy 6101: acetone: polyethylene polyamine: furfural = 10: 10: 2: 2: 2
	MN-8	Grouting	epoxy 6101: acetone: polyethylene polyamine: furfural = 10: 2: 2: 2

2.2. Methods

2.2.1. Lithofacies analysis and testing

Samples YG-5 and YG-6 were selected for petrographic analysis and polished. Under conditions of 25°C and 30% relative humidity, thin sections were observed using a Zeiss Axioskop 40 microscope to identify the microstructure of the rocks, including mineral composition, pore characteristics, and cement properties.

2.2.2. Morphology analysis

Samples MN-1, MN-5, YG-1, and YG-3 were observed using a Keyence VHX-6000 digital microscope (Keyence, Osaka, Japan), and micrographs were captured under visible light using an imdegradation system. Microstructural and elemental analyses were performed using a cold-field scanning electron microscope (Regulus 8100, Hitachi, Japan) equipped with an energy dispersive spectrometer (EDS). Without any pretreatment, the four epoxy resin samples were cut into small pieces (10×10×1 mm^3) for

gold sputtering, fixed with conductive double-sided tape, and then imaged and analyzed at 15 kV. The working distance ranged from 12 to 14.3 mm, and the magnification ranged from 1000× to 2500×.

2.2.3. Nanoindentation analysis

The mechanical properties of samples MN-1, MN-5, YG-1, and YG-3 were measured using a nanoindenter (HYSITRON TI 980 Brook, USA). The elastic modulus and hardness were obtained by applying a maximum load of 2 mN to each coating sample using a Berkovich indenter. Each sample was indented at least eight times, and the final results were calculated as the average of the measurements.

2.2.4. Fourier Transform Infrared Spectroscopy (FTIR)

A Fourier transform infrared spectrometer (Nicolet 6700, Thermo Fisher Scientific, USA) was used for FTIR analysis of samples MN-4, MN-8, YG-7, and YG-3. The test range was from 4000 cm^{-1} to 500 cm^{-1}, with a resolution of 4 cm^{-1}. The OMNIC and ORIGIN software packages were used to process the infrared spectral data.

2.2.5. Thermal stability analysis

Thermal stability was analyzed by thermogravimetric analysis coupled with infrared spectroscopy (TGA-FTIR), for the TGA-FTIR experiment, samples MN-4, MN-8, YG-4, and YG-7 were tested using a synchronous thermal analyzer (STA 449F3, Germany). Approximately 2 mg of each sample was heated from room temperature to 900°C at a heating rate of 10°C /min under an argon atmosphere. The main weight loss temperature range, residual mass percentage, weight loss termination temperature, and other parameters were determined. The volatile gases generated at high temperatures were transferred through a heated pipeline into the gas cell of a coupled Fourier transform infrared spectrometer (VERTEX 70v, Brook, USA), which operated over a test range of 4000 cm^{-1} to 500 cm^{-1} with a resolution of 4 cm^{-1}.

3. Results and discussion

3.1. Lithofacies analysis

Microscopic observation of the rock slices (Fig. 2) reveals a massive sandstone texture composed of quartz, feldspar, mica, and interstitial materials, with pore-filling cementation as the dominant type consistent with previous studies on the Yungang Grottoes [13].

3.2. Microscopic observation

This suggests that the smooth surface layer had been thinned or degraded to such an extent that the EDS signal was dominated by the underlying rock substrate rather than by organic matter; accordingly, this spectrum is markedly different from that of the intact organic coating shown in Fig. 3(h).

SEM imageing revealed that the microstructure of the samples comprised smooth regions and rough filler particles. EDS results further indicated that residual residual organic matter in the field grouting samples was relatively depleted. Consequently, the spectrum obtained from the apparently smooth region (Fig. 3(f))—which would be expected to correspond to the epoxy matrix—instead showed numerous elements associated with inorganic minerals, with oxygen content significantly higher than that in the rough filler region (Fig. 3(e)). This suggests that the smooth surface layer had been thinned or degraded to such an extent that the EDS signal was dominated by the underlying rock substrate rather than by organic matter.

Figure 4 presents microscopy images of the field grouting and coating materials in Cave 16, captured at 200× magnification. In regions corresponding to those examined by SEM, it can be observed that the black, shiny material correspond to aged epoxy, while the brown material represents either rock or a filler such as calcium carbonate. The two materials are in close contact, suggesting intimate interfacial bonding. Comparison with the simulated samples confirms that the darkening of the field coating samples is attributable to material ageing.

(a): Field grouting sample; (b): Simulated grouting sample; (c): Field coating sample; (d): Simulated coating sample; (e): EDS spectrum of field grouting sample at 500-24h-24; (f): EDS spectrum of field grouting sample at 500-24h-26; (g): EDS spectrum of field coating sample at 500-24h-19; (h): EDS spectrum of field coating sample at 500-24h-21

(a): Field grouting sample; (b): Simulated grouting sample; (c): Field coating sample; (d): Simulated coating sample

3.3. Nanoindentation

The nanomechanical properties of the field and simulated coating and grouting samples are summarized in Fig. 5. As shown in Figure S1 (Supplementary Information), the maximum indentation depth of the field samples increased relative to that of the simulated counterparts, indicating reduced resistance to deformation [14]. Compared with the simulated samples, the field coating exhibited decreases in hardness and elastic modulus of 73.91% and 19.85%, respectively, whereas the field grouting showed a 12% decrease in hardness but a 32.56% increase in modulus. These divergent trends may be attributed to the higher filler content in the field grouting samples—resulting from sampling of compositionally heterogeneous regions—or to differences in the extent of degradation between the two materials.

In polymer science, hardness generally reflects the elastic stiffness and intermolecular interactions of molecular chains, whereas the elastic modulus is indicative of crosslink density or chain stiffness [15]. During epoxy degradation, changes in mechanical properties are governed by the competing processes of chain scission and further crosslinking. In the early stage of ageing, both processes coexist: chain scission causes a decrease in hardness, while additional crosslinking leads to an increase in modulus. In the advanced stage, crosslinking ceases and chain scission becomes dominant, resulting in a

progressive decline in both modulus and hardness. An increase in free radicals results in a greater number of micro-defects [16], which reduce both hardness and elastic modulus.

The field coating material exhibits a concurrent decrease in both hardness and modulus (Fig. 5). This is attributed to its greater exposure to oxygen and light at the surface. By contrast, the field grouting sample exhibits modest decrease in hardness but an increase in modulus. It is possible that the sample remains in the early stage of degradation in which crosslinking-induced stiffening dominates the ageing process.

(a) Hardness and (b) elastic modulus of field samples and simulated samples.

3.4. FTIR spectroscopy

The field and simulated coating and grouting samples were characterized by FTIR spectroscopy. The infrared spectra are shown in Fig. 6, and the peak assignments are listed in Table 2. The spectra of the simulated coating and grouting both exhibit characteristic bands at 1249 cm^{-1} and 828 cm^{-1}, attributed to the symmetric and asymmetric C–O–C stretching vibration [17]. The two spectra are similar; however, the grouting sample shows an additional peak at 885 cm^{-1}, assigned to the furan ring in furfural [18, 19].

Comparison of the infrared spectra of the field and simulated coating materials (Fig. 6(a)) reveals marked differences. Relative to the simulated sample (black curve), the field sample (red curve) shows the disappearance of the phenoxy stretching band at 1034 cm^{-1} [20, 21] and the symmetric C–O–C stretching peak at 1249 cm^{-1} [22]. Meanwhile, the ester band at 1112 cm^{-1} increases in intensity [17], and a carbonyl band appears at 1722 cm^{-1}, indicating oxidative degradation and possible conversion of phenoxy groups to ester functionalities. Furthermore, the stretching vibrations of the benzene rings at 1608 cm^{-1} and 1507 cm^{-1} decrease in intensity [23, 24], suggesting oxidation of the aromatic rings and a consequent reduction in aromaticity [21].

In the simulated coating sample, the intensities of the methyl bands at 2964 cm^{-1} and 2870 cm^{-1} are similar to those of the methylene bands at 2931 cm^{-1} and 2814 cm^{-1}. In contrast, the field sample exhibits weakened methyl absorption, and the isopropyl band at 1179 cm^{-1} disappears [25], leaving only methylene bands at 2917 cm^{-1} and 2849 cm^{-1} [26]. This indicates extensive reaction of the isopropyl groups, consistent with the reported mechanism involving cleavage of isopropyl groups from the aromatic rings, free-radical formation, and oxidation [27]. These reactions produce ketones and other carbonyl-containing species, which are considered the primary cause of material darkening [28]. Figure 6(b) shows that the ageing process of the grouting material is essentially analogous to that of the coating, involving chain scission and subsequent oxidative reactions.

Notably, many main-chain features, such as C–O–C stretching modes, persist in the spectrum of the field grouting material in the 900 cm^{-1} and 1034 cm^{-1} region, indicating a relatively low extent of degradation. In contrast, both the phenoxy characteristic band and the benzene-ring stretching vibrations (1608 cm^{-1} and 1507 cm^{-1}) disappear in the spectrum of the field coating material, indicating substantial

degradation of the aromatic structure. Given the inherent stability of benzene ring, this finding suggests that the epoxy coating material has undergone severe degradation, significantly exceeding that of the grouting material.

In summary, the observed spectral changes — specifically the loss of phenoxy and isopropyl bands and the formation of carbonyl groups — are consistent with the free radical mechanism reported in the literature [14, 21]. The epoxy coating material, being directly exposed at the surface, exhibits a high extent of degradation and appears to be approaching the end of its service life.

Table 2
Assignments and attribution of FTIR spectra of coating and grouting materials

Wavenumber(cm^{-1})		Assignment
Coating	**Grouting**	
3445	3445	v(O-H)
2964、2870	2964、2870	v($-CH_3$)
2917, 2849	2932, 2853	v($-CH_2-$)
1722	1723	v(C = O)
1608, 1507	1607, 1509	v(C = C) (aromatic ring)
1249	1249	v_{sym}(C-O-C) (aryl)
1112	1112	v(O-C-C) (alkyl)
1179	1179	v(CH-$(CH_3)_2$)
1034	1034	v(C-O-C)
828	830	v_{asym}(C-O-C)
	885	v_{asym} (C-H)
v:stretching, δ: bending		

(a) Coating materials; (b) Grouting materials.

3.5. Thermogravimetric analysis

The TGA results are presented in Fig. 7. The initial decomposition temperatures of the field and simulated coating samples are 200°C and 299°C, respectively, whereas those of the grouting materials are 100°C and 248°C, respectively. These data indicate that the thermal stability of the field samples is lower than that of the simulated counterparts.

Derivative thermogravimetric (DTG) results show that the simulated samples each exhibit a single-stage profile with a bimodal peak centered near 400°C. In contrast, the field samples display a more complex, multistage degradation pattern.

The first stage, occurring at approximately 121°C, is observed exclusively in the field grouting sample (Fig. 7(d)). This stage may be attributed to the volatilization of low-molecular-weight degration products or adsorbed moisture, potentially reflecting prolonged exposure to the humid microenvironment within the rock fractures of the Yungang Grottoes.

In the second stage (300 ℃ – 360 ℃), the maximum mass-loss-rate temperature (T_{max}) of the field coating is approximately 300 ℃, while that of the field grouting is 333 ℃. The lower T_{max} values of the field coating samples suggest that ageing has introduced more thermally labile structures into the resin network, the field coating samples were more severely aged [29]. Considering the decomposition temperatures of the simulated and field grouting samples are comparable, this discrepancy indicates that the coating has undergone a more severe degree of degradation than the grouting.

The third stage (410 ℃ -510 ℃), corresponds to the decomposition of the main polymeric backbone. The field coating and grouting samples exhibit T_{max} values of 480°C and 506°C, respectively, possibly owing to the presence of more highly crosslinked residual structures [30].

Beyond 510°C, the rate of mass loss gradually decreases. In the fourth stage (> 650 ℃), the residual mass loss observed for the field samples may be attributed to the decomposition of inorganic minerals or fillers present in the materials.

(a): TGA curve of coating samples; (b): DTG curve of coating samples; (c): TGA curve of grouting samples; (d): DTG curve of grouting samples

3.6. TG-FTIR analysis of pyrolysis products

According to the DTG results, excluding the minor mass-loss stages below 120 ℃ and above 600 ℃, two principal stages are associated with the pyrolysis of the epoxy resin: one ranging from 300 ℃ to 400 ℃ and the other from 400 ℃ to 550 ℃. We focused on these two main pyrolysis stages of the organic matter, and the infrared spectra of the evolved gases are shown in Figs. 8 and 9.

The TG-FTIR results reveal substantial differences between the simulated and field samples, indicating severe degradation of the epoxy resin in Cave 16. The three-dimensional evolved gas spectra of the simulated coating and grouting samples pyrolyzed from 100°C to 800°C under an argon atmosphere (Figs. 8(a) and 9(a)) indicate that volatile components were continuously released during heating. The pyrolysis temperatures and products of the two simulated materials were similar (Figs. 8(c) and 9(c)), primarily including water, hydrocarbons, CO_2, aromatic products such as benzene, and various gas mixtures containing isopropyl-bearing species. Compared with the first pyrolysis stage (357–359°C), the second pyrolysis stage (410–416°C) produced a greater abundance of aromatic compounds.

Furthermore, the simulated grouting sample produced more aromatic products during pyrolysis, which can be explained by the enhancing effect of furfural on aromaticity.

The evolved gas spectra of the field samples (Figs. 8(b) and 9(b)) exhibited a markedly reduced diversity of pyrolysis products.

During the first pyrolysis stage (300°C) of the field coating, the pyrolysis products included water, hydrocarbons, CO_2, and various gas mixtures containing benzene (Fig. 8(d)). In the second pyrolysis stage (480°C), the pyrolysis products were predominantly hydrocarbons (2933 cm^{-1}), indicating that the natural ageing products of the epoxy coating material are predominantly an aliphatic polymeric residue [31]. Both simulated samples exhibit a T_{max} around 416°C, with pyrolysis products potentially including peroxides, carboxyl-containing species, and various hydrocarbons [32]; aromatic structures are degraded during this stage [33]. Additionally, the CO_2 generated at 687°C may be attributed to the pyrolysis of carboxylate substances derived from inorganic minerals or formed during the ageing of the epoxy resin [34].

During the first pyrolysis stage (333°C) of the field grouting, the products included formaldehyde, acetone, and ethers (Fig. 9(d)), with weak hydrocarbon signals. In the second pyrolysis stage (506°C), the products comprised a small amount of hydrocarbons and predominantly CO_2. This indicates that the natural ageing products of the epoxy grouting material retained more reactive functional groups such as isopropyl and carbonyl moieties, reflecting a lesser extent of degradation [35, 36]. Throughout the heating process, the CO_2 signal was disproportionately intense, which may be attributed to sample inhomogeneity and high inorganic matter content.

In summary, based on the gases released during pyrolysis, the natural ageing final products of the epoxy resin (coating material) are speculated to be aliphatic polymeric residues, possibly accompanied by carboxylate species. By contrast, the intermediate degradation products of the epoxy resin (grouting material) retain carbonyl and isopropyl groups. As the ageing products are essentially consistent with the literature reported by Buch et al. [17], it is speculated that isopropyl reactions, main-chain breakage, and subsequent peroxide radical reactions constitute the primary ageing reaction pathways.

(a): Three-dimensional evolved gas spectra of simulated samples at different temperatures; (b): Three-dimensional evolved gas spectra of field samples at different temperatures; (c): FTIR spectra of simulated samples at specific temperatures; (d): FTIR spectra of field samples at specific temperatures

(a): Three-dimensional evolved gas spectra of simulated samples at different temperatures; (b): Three-dimensional evolved gas spectra of field samples at different temperatures; (c): FTIR spectra of simulated samples at specific temperatures; (d): FTIR spectra of field samples at specific temperatures

4. Conclusions

Research on the long-term performance of organic cultural heritage conservation materials under actual environments remains limited. Lever ageing the early application of epoxy materials at the Yungang Grottoes, this study collected epoxy grouting and coating materials that had undergone approximately 50 years of natural ageing in Cave 16. The micro-morphology, mechanical properties, thermal stability, and chemical structure of these materials were comprehensively characterized using microscopy, nano-indentation, thermogravimetry, and FTIR. The natural ageing products were inferred, and the service state and ageing mechanism of the epoxy materials were discussed.

Collectively, the results demonstrate that the epoxy materials have undergone severe degradation. The coating material exhibits a higher degree of ageing due to greater exposure to oxygen and light. Microscopic observation revealed darkening of both the coating and grouting materials. Nanoindentation indicates a reduction in hardness for both materials; however, the modulus of the grouting increased, whereas that of the coating decreased. This discrepancy may be attributed to the presence of cementitious filler or to differences in the degree of degradation. FTIR and TG-FTIR analyses revealed substantial differences between the simulated and field samples. The natural ageing final products of the coating material are inferred to be aliphatic polymeric residues, possibly accompanied by carboxylate species, whereas the ageing products of the grouting material represent intermediate degradation products retaining carbonyl and isopropyl groups, reflecting a lesser extent of degradation. The carbonyl groups generated during ageing are the primary cause of material darkening.

Despite limited field specimens owing to strict sampling restrictions, comparison with simulated samples enabled a tentative elucidation of the material ageing mechanism. Under cave environments and long-term natural ageing conditions, it is speculated that the ageing of epoxy materials essentially follows the free-radical mechanism reported in the literature.

The rarity of conservation materials subjected to half a century of in situ ageing underscores the exceptional value of this dataset. Nevertheless, to further clarify the reaction mechanisms—particularly those operative in the early stages of degradation—future research must endeavor to collect specimens spanning a broader spectrum of ageing states.

Declarations

Authors' contributions:

Conceptualization, X. He; Data acquisition, S.X. Qiao and Q. Wang; Funding acquisition, S.X. Qiao and X. He; Methodology, X. He and S.X. Qiao; Resources. S.X. Qiao, D. Yan, and X. Bai; Supervision, X. He; Writing - original draft, X. He and Q. Wang; Writing - review & editing, S.X. Qiao and X. He. All authors read and approved the final manuscript.

Competing interests:

The authors declare no competing interests.

Acknowledgements:

This work was financially supported by the Fundamental Research Program of Shanxi Province in 2025(202503011272009), Cultural Relics Science and Technology Project of the National Cutural Heritage Administration (grant number 2023ZCK010, 2023ZCK005), and Research Project of Shanxi Provincial Cultural Relics Bureau, grant number 2024KT24.

Declaration of Generative AI and AI-assisted technologies in the writing process:

During the preparation of this work the authors used ChatGPT and DeepSeek in order to check grammar, spell, academic phrasing, and terminology. After using this tool, the authors reviewed and edited the content as needed and take full responsibility for the content of the publication.

References

1. Wu Qiaoyun. Where Are the Northern Wei Musical Joys? They Sing Daily in the Yungang Grottoes for a Millennium: A Study of Northern Wei Music Embodied in the Musical Instrument Images of the Yungang Grottoes. Huangzhong: J Wuhan Conservatory Music. no. 4, 55–65(2017).
2. Kotlik P, Justa P, Zelinger J. The application of epoxy resins for the consolidation of porous stone. Stud Conserv. 1983;28:75–9.
3. Tang Z, Liu X, Feng X. Research progress on epoxy resins in cultural heritage conservation. Polymers. 2025;17:1747.
4. Selwitz CM. The use of epoxy resins in field projects for stone stabilization. *MRS Online Proc. Libr.* 267, 925 (1992).
5. Xie T. Improvements in the application of epoxy resin in the reinforcement project of the Yungang Grottoes. In *Cultural Relics Protection Technology (1981–1991)*, 261–263 (2010).
6. Selwitz C. Epoxy Resins in Stone Conservation. Getty; 1992.
7. Zahra Y, Djouani F, Fayolle B, Kuntz M, Verdu J. Thermo-oxidative aging of epoxy coating systems. Prog Org Coat. 2014;77:380–7.
8. Liu J, Wang H, Zhang W, et al. Mechanistic insights into catalysis of in-situ iron on pyrolysis of waste printed circuit boards: Comparative study of kinetics, products, and reaction mechanism. J Hazard Mater. 2022;431:128612.
9. Galant C, et al. Thermal and radio-oxidation of epoxy coating. Prog Org Coat. 2010;69:322–9.
10. Dai S, Song P, Jiao Z, Ren S, Lin R. Synthesis, properties and thermal degradation mechanism of bisphenol A-based polyarylates capped with p-tert-butylphenol. J Therm Anal Calorim. 2023;148:4211–21.
11. Wu Y, et al. New insights into brominated epoxy resin type WPCBs pyrolysis mechanisms: Integrated experimental and DFT simulation studies. Sci Total Environ. 2024;912:169610.

12. Tesser E, Lazzarini L, Bracci S. Investigation on the chemical structure and ageing transformations of the cycloaliphatic epoxy resin EP2101 used as stone consolidant. J Cult Herit. 2018;31:72–82.
13. Yang X, et al. The mechanisms of salt weathering responsible for sandstone deterioration in the Yungang Grottoes, China. Eng Geol. 2025;350:107989.
14. Wu F et al. IEEE,. Cyanate ester/epoxy co-curing system with thermal stabilizers for high temperature stability. In *2018 IEEE 68th Electronic Components and Technology Conference (ECTC)* 2237–2242 (2018).
15. Wan X, Demir B, An M, Walsh TR, Yang R. Thermal conductivities and mechanical properties of epoxy resin as a function of the degree of cross-linking. Int J Heat Mass Transf. 2021;180:121821.
16. Liu S, et al. Formation of environmentally persistent free radicals on microplastics under UV irradiations. J Hazard Mater. 2023;453:131277.
17. Smith BC. The infrared spectra of polymers V: epoxies. Spectroscopy. 2022;3:17–9.
18. Araújo CF, et al. Crystal structure of poly(trimethylene 2,5-furandicarboxylate) redux – a new model supported by computational spectroscopy. Polym Chem. 2024;15:4349–63.
19. Thiviyanathan VA, et al. Detection of 2FAL furanic compound in transformer oil using optical spectroscopy method and verification using morse oscillation theory. IEEE Access. 2020;8:76773–9.
20. Goyanes SN, König PG, Marconi JD. Dynamic mechanical analysis of particulate-filled epoxy resin. J Appl Polym Sci. 2003;88:883–92.
21. Yan H, Wang P, Li R, Cheng Z, Sun S. Degradation behaviour of encapsulated assemblies of epoxy resin under accelerated thermal cycling. Int J Polym Anal Charact. 2022;27:180–94.
22. Smith BC. Infrared Spectroscopy of Polymers X: Polyacrylates. *Spectroscopy.* 38, 10 – 14 (2023).
23. Odegaard N, et al. Pine pitch: new treatment protocols for a brittle and crumbly conservation problem. Objects Spec Group Postprints. 2014;21:21–41.
24. Martín-Ramos P, Fernández-Coppel IA, Ruíz-Potosme NM, Martín-Gil J. Potential of ATR-FTIR Spectroscopy for the Classification of Natural Resins. Biol Eng Med Sci Rep. 2018;4:3–6.
25. Yosief HO, Sarker MI, Bantchev GB, Cermak SC, Biresaw G. Isopropyl-branched lard and its potential application as a bio-based lubricant. Lubr Sci. 2024;36:104–18.
26. Wang Z, et al. Durability study on interlaminar shear behaviour of basalt-, glass- and carbon-fibre reinforced polymer (B/G/CFRP) bars in seawater sea sand concrete environment. Constr Build Mater. 2017;156:985–1004.
27. Wiberg KB, Schaefer H. Chromic acid oxidation of isopropyl alcohol. Oxidation steps. J Am Chem Soc. 1969;91:933–6.
28. Kumar BG, Singh RP, Nakamura T. Degradation of carbon fiber-reinforced epoxy composites by ultraviolet radiation and condensation. J Compos Mater. 2002;36:2713–33.
29. Park CH, Lee SJ, Lee TH, Kim HJ, Lee SW. Characterization of an acrylic pressure-sensitive adhesive blended with hydrophilic monomer exposed to hygrothermal degradation: Assigning cloud point

resistance as an optically clear adhesive for a touch screen panel. React Funct Polym. 2016;100:130–41.

30. Pei Y, et al. Thermal-oxidative degradation of DGEBA/EPN/LMPA epoxy system: Chemical structure and thermal–mechanical properties. Polym Degrad Stab. 2011;96:1179–86.
31. Park KB, Kim JS. Pyrolysis products from various types of plastics using TG-FTIR at different reaction temperatures. J Anal Appl Pyrol. 2023;171:105983.
32. Wang X, Hu Y, Song L, Xing W, Lu H. Thermal degradation mechanism of flame retarded epoxy resins with a DOPO-substituted organophosphorus oligomer by TG-FTIR and DP-MS. J Anal Appl Pyrol. 2011;92:164–70.
33. Qiao Y, et al. Pyrolysis kinetic study and reaction mechanism of epoxy glass fiber reinforced plastic by thermogravimetric analyzer (TG) and TG–FTIR (Fourier-transform infrared) techniques. Polymers. 2020;12:2739.
34. Wang Y, et al. Steam reforming of alcohols and carboxylic acids: Importance of carboxyl and alcoholic hydroxyl groups on coke properties. J Energy Inst. 2021;98:85–97.
35. Luda MP, Balabanovich AI, Camino G. Thermal decomposition of fire retardant brominated epoxy resins. J Anal Appl Pyrol. 2002;65:25–40.
36. Levchik SV, Weil ED. Thermal decomposition, combustion and flame-retardancy of epoxy resins – a review of the recent literature. Polym Int. 2004;53:1901–29.

Figures

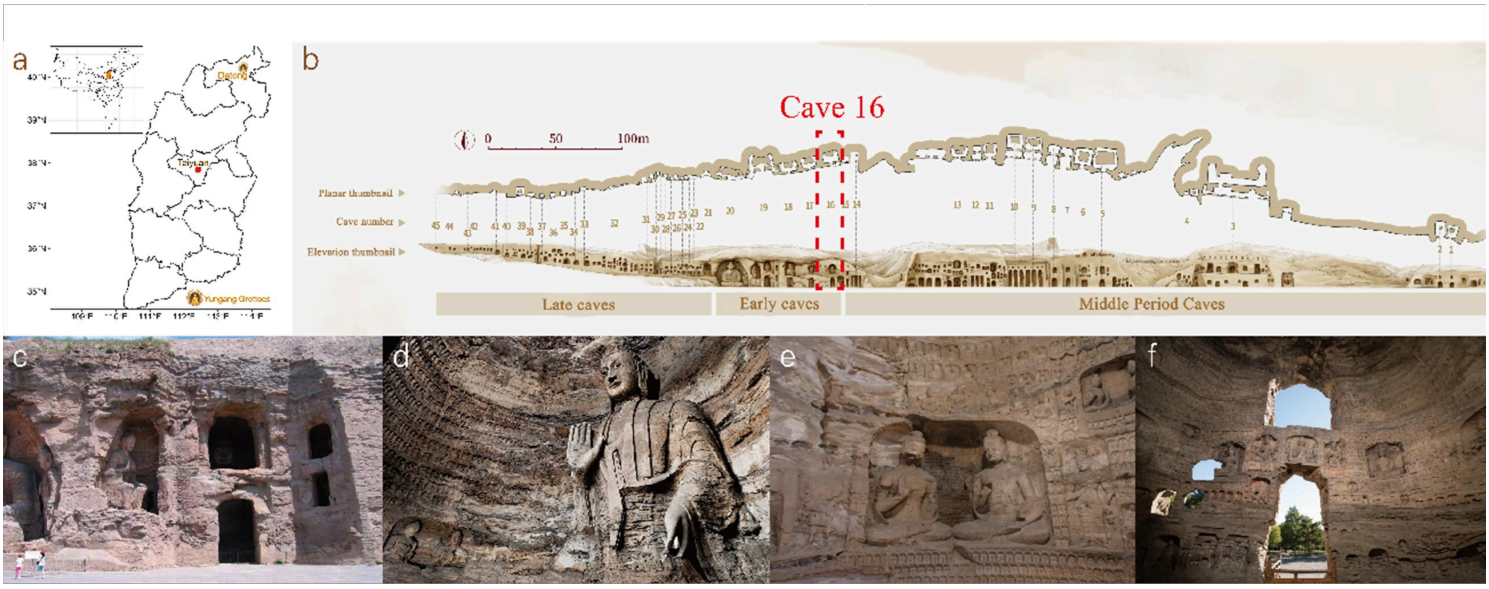


Figure 1

(a): Geographical location of Yungang Grottoes (b): Cave Distribution Map of Yungang Grottoes (c): Cave 16 Elevation Scene Map (d): Cave 16 Main Buddha (e): Cave 16 East Wall Small Buddha (f): Cave 16 South Wall

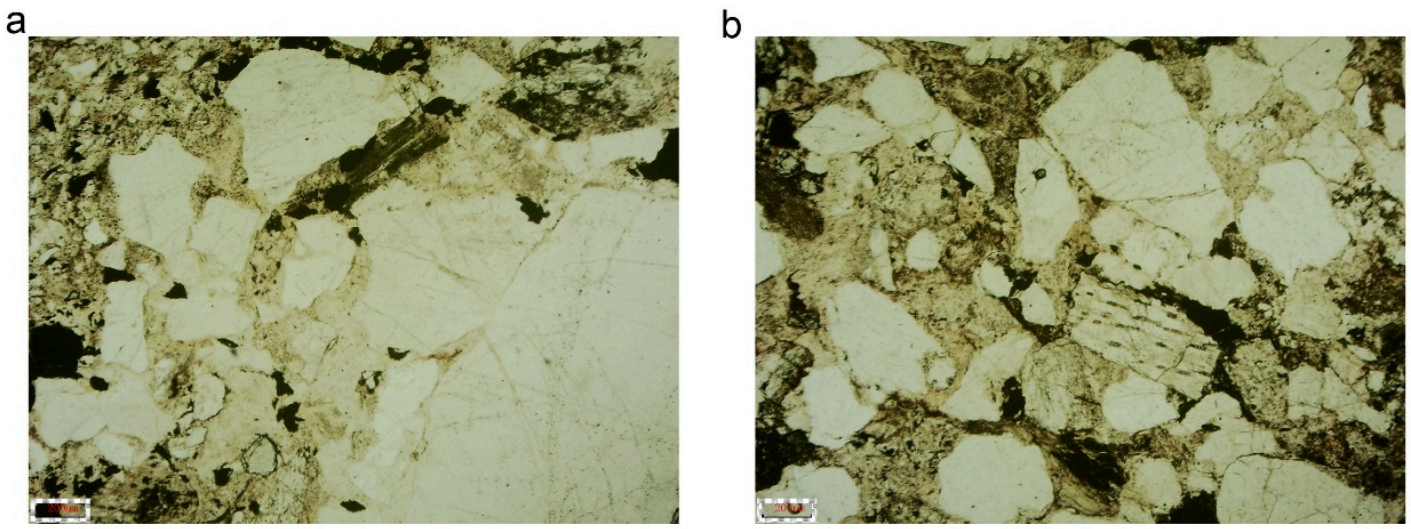


Figure 2

(a) and (b): Lithofacies analysis results of the Yungang Grottoes

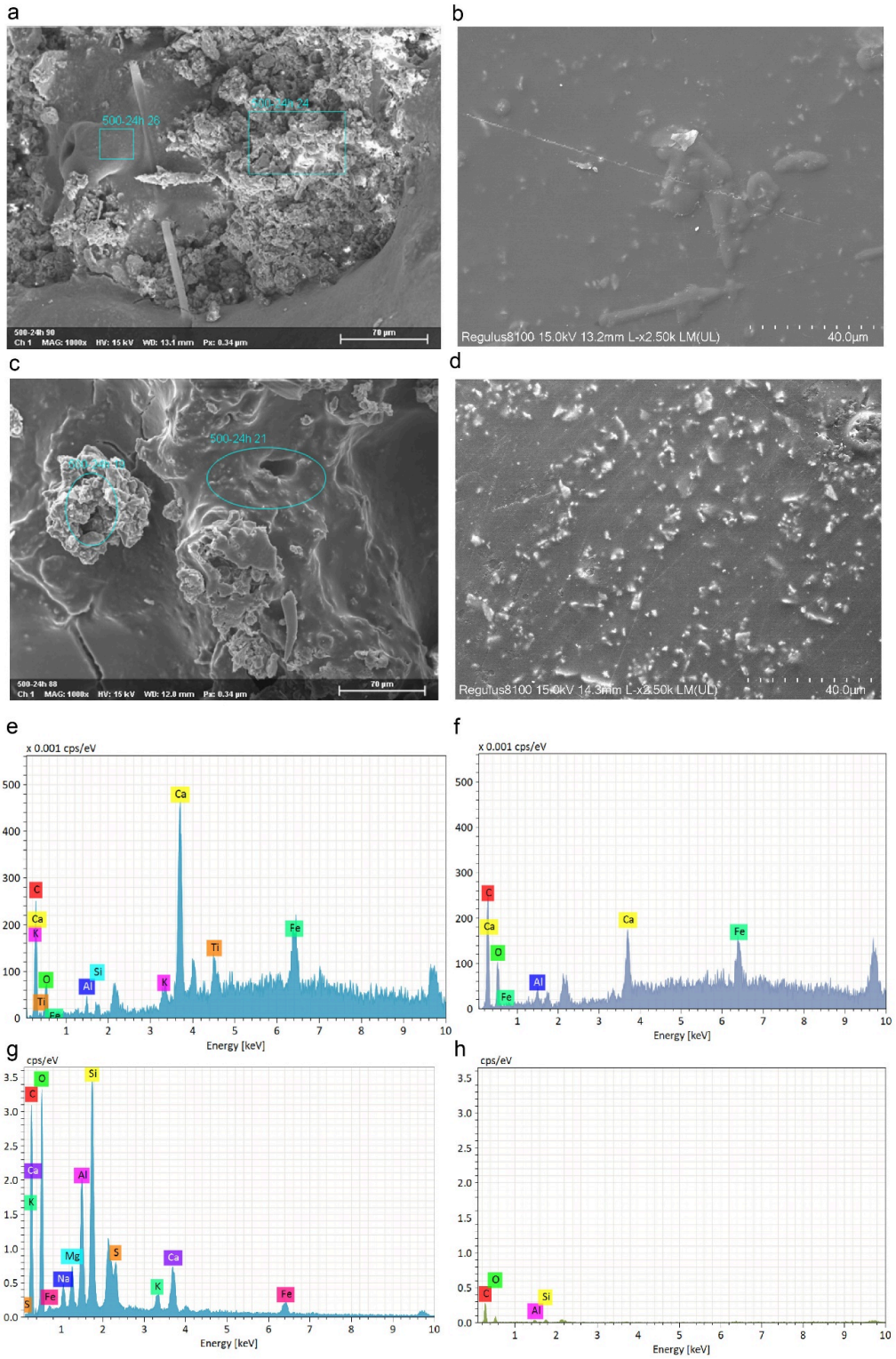


Figure 3

SEM image and EDS spectra of the samples

(a): Field grouting sample; (b): Simulated grouting sample; (c): Field coating sample; (d): Simulated coating sample; (e): EDS spectrum of field grouting sample at 500-24h-24; (f): EDS spectrum of field

grouting sample at 500-24h-26; (g): EDS spectrum of field coating sample at 500-24h-19; (h): EDS spectrum of field coating sample at 500-24h-21

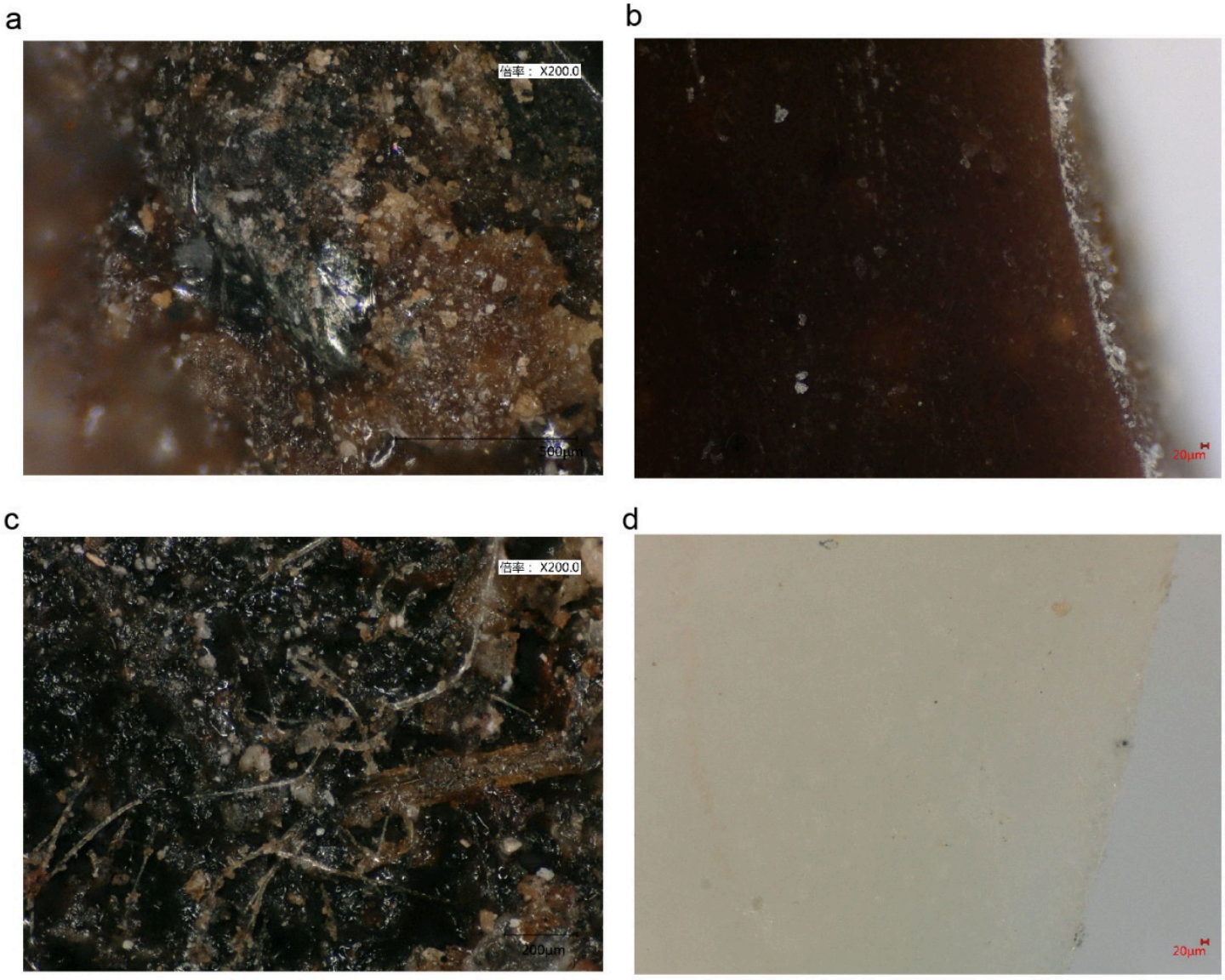


Figure 4

Microscopic images of samples

(a): Field grouting sample; (b): Simulated grouting sample; (c): Field coating sample; (d): Simulated coating sample

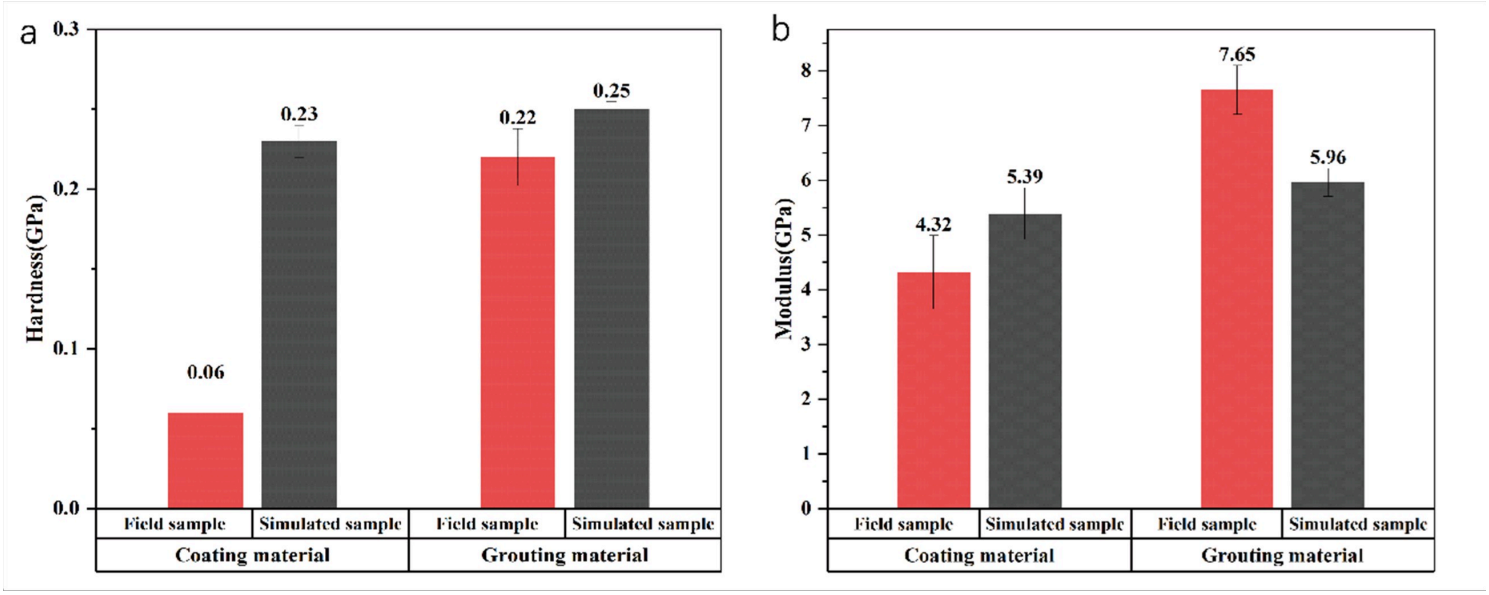


Figure 5

Nanomechanical properties of the field and simulated samples.

(a) Hardness and (b) elastic modulus of field samples and simulated samples.

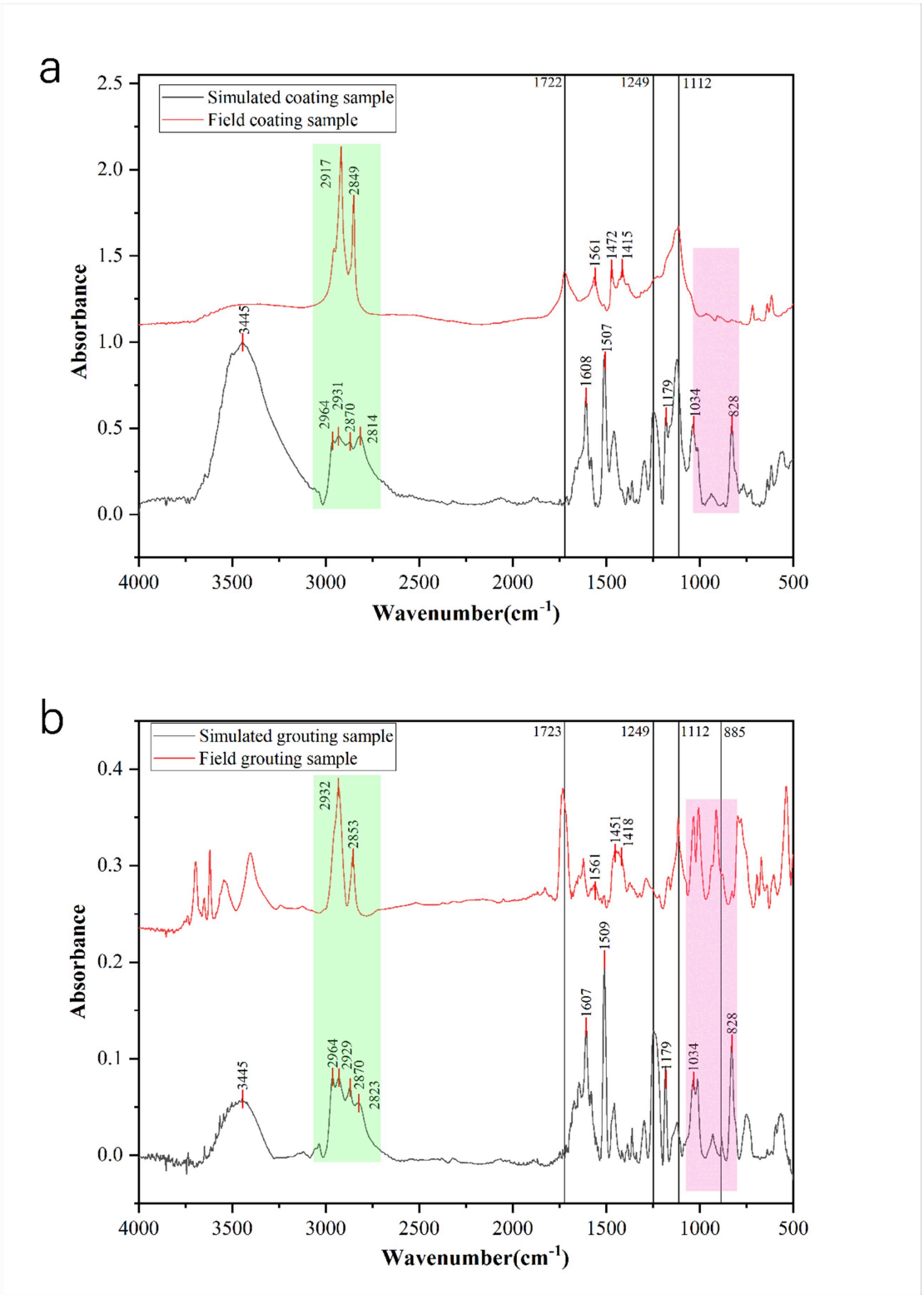


Figure 6

FTIR spectra of the simulated and field samples

(a) Coating materials; (b) Grouting materials.

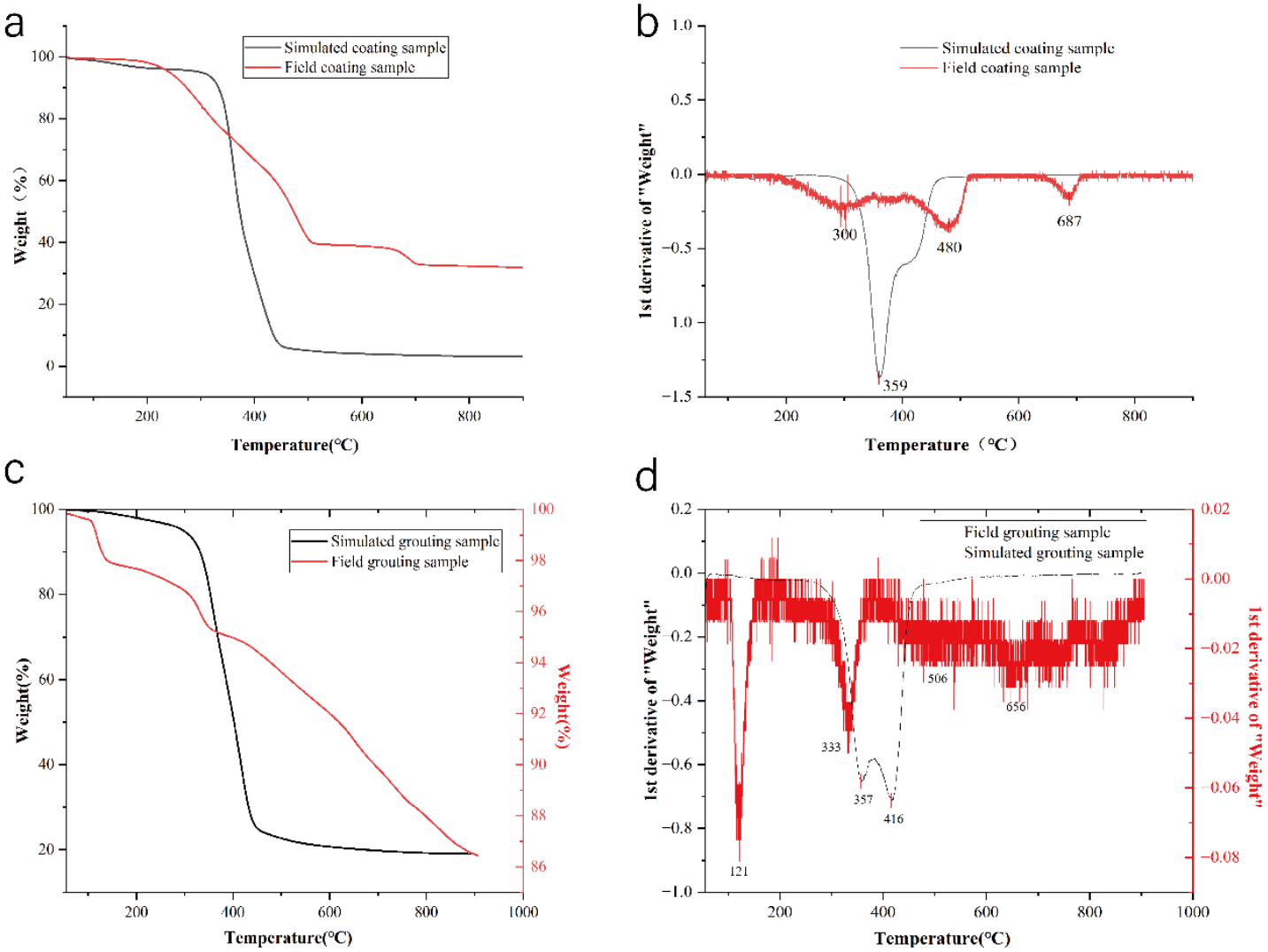


Figure 7

The results of thermogravimetric analysis of field and simulated samples

(a): TGA curve of coating samples; (b): DTG curve of coating samples; (c): TGA curve of grouting samples; (d): DTG curve of grouting samples

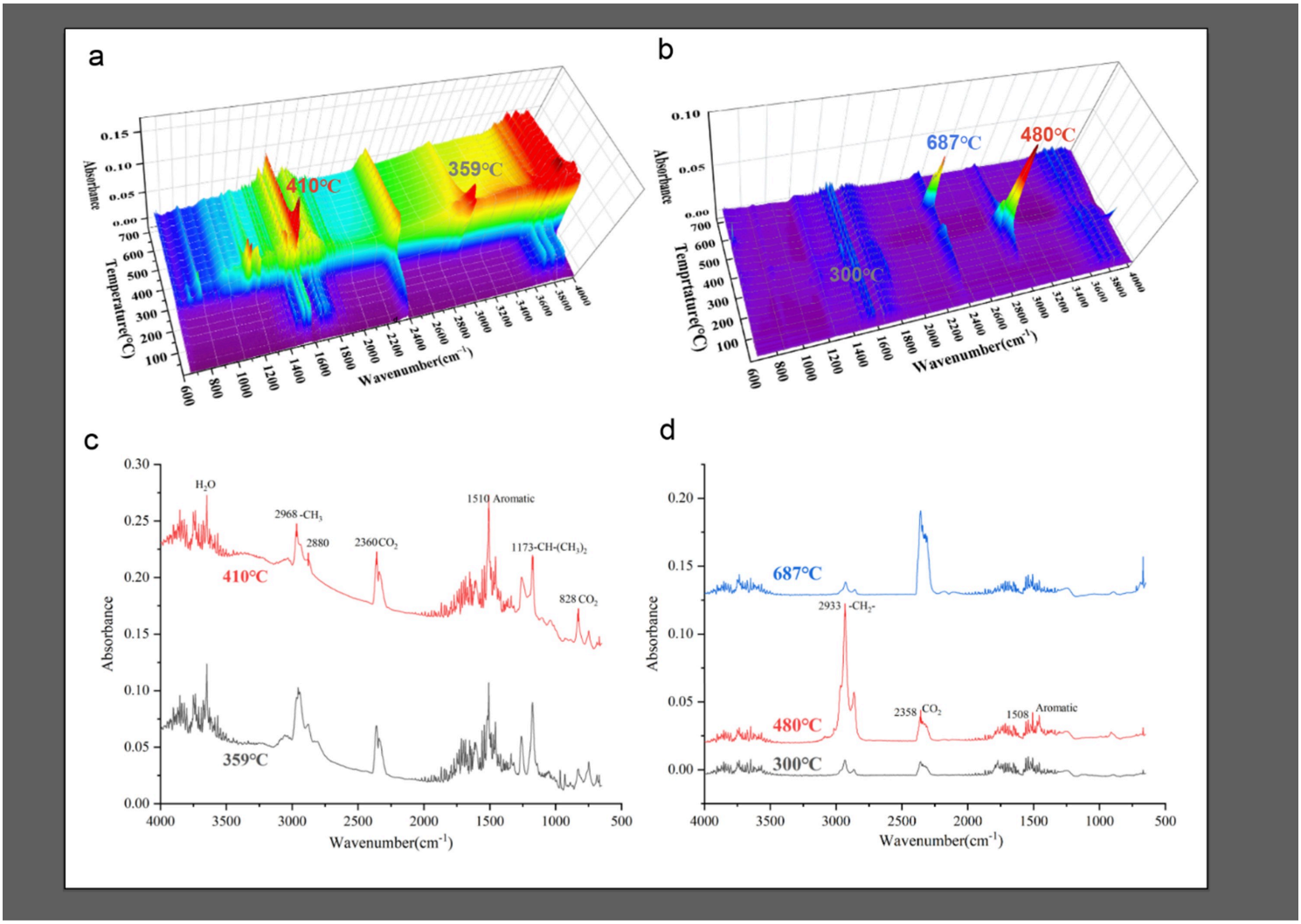


Figure 8

TG-FTIR results for the coating samples

(a): Three-dimensional evolved gas spectra of simulated samples at different temperatures; (b): Three-dimensional evolved gas spectra of field samples at different temperatures; (c): FTIR spectra of simulated samples at specific temperatures; (d): FTIR spectra of field samples at specific temperatures

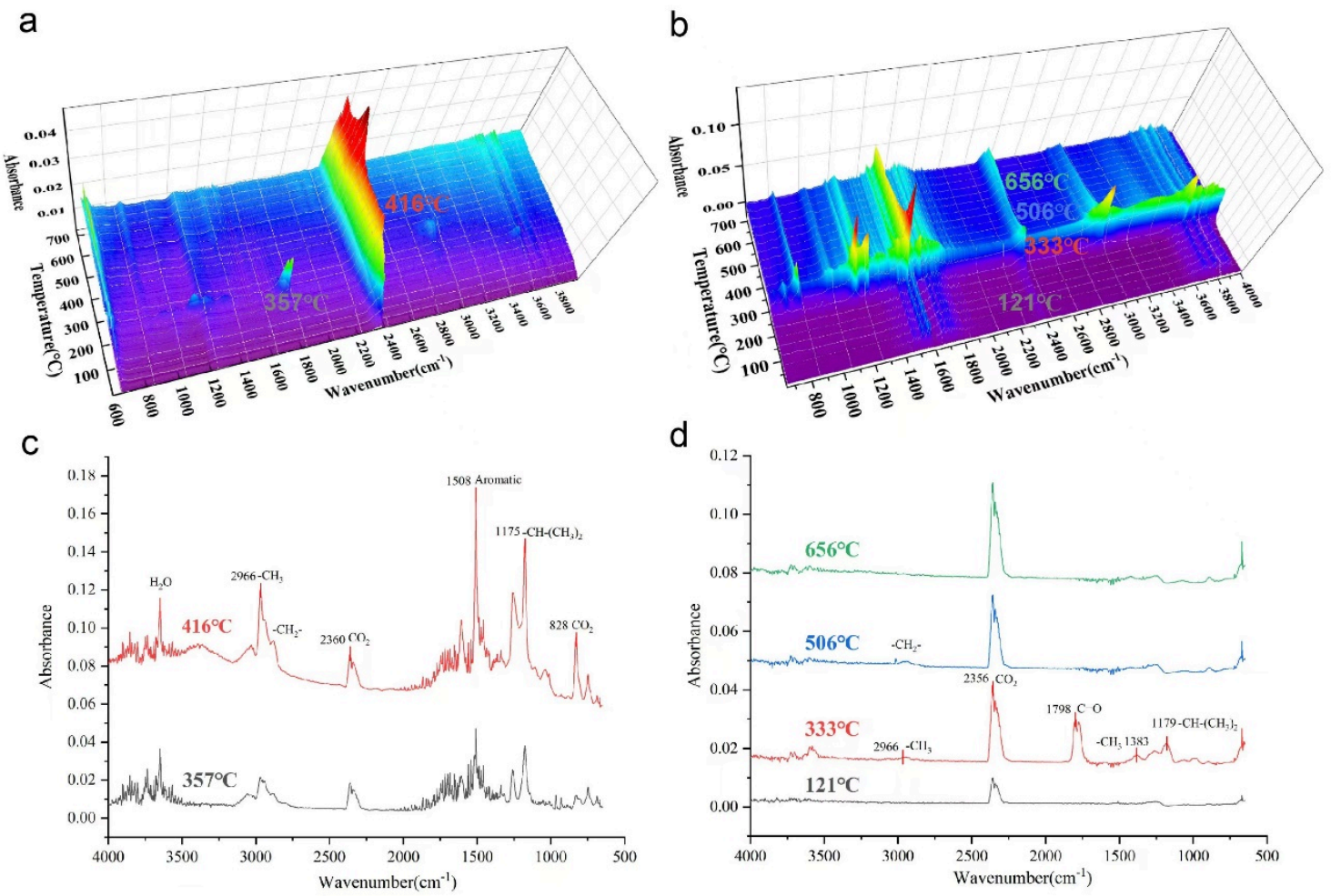


Figure 9

TG-FTIR results for the grouting samples

(a): Three-dimensional evolved gas spectra of simulated samples at different temperatures; (b): Three-dimensional evolved gas spectra of field samples at different temperatures; (c): FTIR spectra of simulated samples at specific temperatures; (d): FTIR spectra of field samples at specific temperatures

Supplementary Files

This is a list of supplementary files associated with this preprint. Click to download.

- Supplementaryinformation.docx